



# Carboxyl-fentanyl detection using optical fibre grating-based sensors functionalised with molecularly imprinted nanoparticles

LiangLiang Liu<sup>a,1</sup>, Fabiana Grillo<sup>c,1</sup>, Francesco Canfarotta<sup>b</sup>, Michael Whitcombe<sup>c</sup>, Stephen P. Morgan<sup>a</sup>, Sergey Piletsky<sup>c</sup>, Ricardo Correia<sup>a</sup>, ChenYang He<sup>a</sup>, Andrew Norris<sup>d,e</sup>, Serhiy Korposh<sup>a,\*</sup>

<sup>a</sup> Optics and Photonics Group, University of Nottingham, Nottingham, UK

<sup>b</sup> MIP Diagnostics Ltd, Bedford, UK

<sup>c</sup> Department of Chemistry, University of Leicester, Leicester, UK

<sup>d</sup> Department of Anesthesiology, Nottingham University Hospitals NHS Trust, Nottingham, UK

<sup>e</sup> Department of Anesthesiology, King Faisal Specialist Hospital and Research Centre, Riyadh, Saudi Arabia

## ARTICLE INFO

### Keywords:

Fentanyl

Optical fibre long period grating

Molecular imprinting

## ABSTRACT

Butyrylfentanyl is a new designer drug reported with growing use and related deaths. Routine toxicological analyses of this novel synthetic opioid drug have not been established yet. This work reports a fibre optic sensor that measures carboxyl-fentanyl which is the major metabolite of butyrylfentanyl presented in blood, providing a promising tool for detecting butyrylfentanyl intoxication. A long period fibre grating (LPG) sensor array operating at phase-matching condition is deployed in combination with a state-of-the-art molecular imprinting technique. Nano-sized molecularly imprinted polymers (nanoMIPs) are synthesised via a solid-phase approach and coated on the surface of an LPG array. An LPG array consists of two parts: a detection and a reference LPG. The former is functionalised with nanoMIPs prior to the measurements, whilst the latter is used to take into account the temperature response of the detection LPG. The developed sensor exhibits a gradual response over increasing concentrations of carboxyl-fentanyl from 0 to 1000 ng/mL with a minimal detected concentration of 50 ng/mL, that corresponds to a wavelength shift of  $1.20 \pm 0.2$  nm. The Langmuir adsorption isotherm is applied to fit the analytical data which reveal a binding constant of  $2.03 \mu\text{M}^{-1}$ . The developed sensor shows high selectivity in detecting carboxyl-fentanyl among other drugs and potential interferents including morphine, cocaine, glucose and albumin. It shows a certain degree of cross-response to fentanyl which shares the same binding sites as carboxyl-fentanyl and therefore can be potentially used to detect fentanyl.

## 1. Introduction

The interest in drug detection is increasing due to high demand in sporting competitions and police investigations. According to the United Nations Office on Drugs and Crime, nearly five percent of the global adult population regularly consumed prohibited drugs (world drug report 2015, UNODC).

Opioid-related deaths have been reported worldwide as the biggest contributor to drug-related deaths (66% of drug deaths in 2017) (Rubin, 2017; Kimber et al., 2019) where both prescription and non-prescription (illicit) opioid are responsible for these deaths. Repeated warnings were emitted by the EMCDDA particularly in relation to fentanyl diffusion in

different areas of Europe as well as the presence of new formulations of fentanyl analogues, with some of them up to 10,000 times more potent than morphine (O'Donnell et al., 2017).

In addition to the already known and scheduled substances, new psychoactive substances are continuously being brought to the market, rising serious worries as their pharmacological and toxicological effects are mostly unknown (A and European Drug Repo, 2017), in addition to the lack of routine testing in standard toxicology analysis (Oldenhof et al., 2020).

Between 2012 and 2017, more than a dozen additional fentanyl analogues have entered the illicit opioid market. Some of these analogues have been re-discovered by traffickers from research work

\* Corresponding author.

E-mail address: [s.korposh@nottingham.ac.uk](mailto:s.korposh@nottingham.ac.uk) (S. Korposh).

<sup>1</sup> These authors contributed equally to this work.

carried out between the 1960s and 1990s. These substances were described in the scientific literature, but never developed into pharmaceutical products. Examples include acetylfentanyl, butyrfentanyl, furanylfentanyl, and ocfentanil (Crime, 2017).

Butyrylfentanyl is an analogue of fentanyl with an N-butyryl group replacing the N-propionyl group of fentanyl (modified fentanyl). It is a novel synthetic opioid as a substitute for prescription opioid with potency seven times that of morphine and 0.13 time of fentanyl (Armenian et al., 2018), temporarily scheduled as Schedule I substance under the Controlled Substances Act in 2016 (Drug Enforcement Administ, 2016). It is not approved for medical use, but it is being used for recreational purpose with cases of fatal overdoses reported (Le and Alzghari, 2019). As most of the designer drugs, the actual extent of abuse and mortality associated with butyrylfentanyl is not known due to the lack of routine toxicological analyses (Organization, 2016).

The metabolism of butyrylfentanyl is studied by Steuer et al. with authentic blood and urine samples from a fatal intoxication case. It reveals that hydroxylation of the butanamide side chain followed by oxidation to the carboxylic acid is the major metabolic pathway of butyrylfentanyl *in vivo* (Steuer et al., 2017). A similar conclusion is drawn by Staeheli et al. who concluded that carboxyl-fentanyl is identified as one of the two most abundant metabolites (Staeheli et al., 2016). It is therefore, of great interest to detect carboxyl-fentanyl in blood samples to determine intoxication of butyrylfentanyl, especially considering that the misuse of novel synthetic opioids, including butyrylfentanyl, has become a new deadly trend epidemically (Prekupec et al., 2017). The global drugs of abuse testing market in 2017 has been evaluated at \$4,443.9 million by the United Nations Office on Drugs and Crime (Drugs of Abuse Testing Ma, 2018), and is estimated to swell up to \$6,781.6 million by 2025. This highlights a rising need for reliable, quick, and robust methods of detection for drugs of abuse (Shaw and Dennany, 2017; Campuzano et al., 2018; Wren et al., 2014). The current developed methods to measure fentanyl or fentanyl-analogues such as gas-liquid chromatography (Kowalski et al., 1987), surface-enhanced Raman spectroscopy (Haddad et al., 2018), thermal desorption direct analysis based on real time mass spectrometry (TD-DART-MS) and ion mobility spectrometry (IMS) (Sisco et al., 2017). Despite the fact that these techniques have successfully been applied in many laboratories, this technology is not always readily available for real time routine police checks and often requires technical expertise. The instruments also cannot be scaled down into a portable device for *in situ* detection in forensic or real time detection for medical purposes. In parallel to the quantitative methods just described, semi-quantitative methods have been used in hospitals as routine urine toxicology screens using enzyme-mediated immunoassays such as enzyme linked immunosorbent assay (ELISA) (Tiscione and Wegner, 2017; Wang et al., 2011) and radioimmunoassay (Michiels et al., 1977). However, despite the many advantages, numerous well-known disadvantages need to be considered when immunological/enzymatic elements are involved. Refrigeration is required for transport and storage, and the production of antibodies is characterised by a long manufacture period, 6–9 weeks in the case of polyclonal antibodies and cost is a further problem to consider (Leenaars and Hendriksen, 2005). Ultimately, because of these issues, neither mass spectroscopy nor immunoassays are ideal for real time blood monitoring in clinical applications, or for *in situ* forensic tests. It would therefore be beneficial to develop a low cost, easy to use, point of care sensor.

Molecularly imprinted polymeric nanoparticles (nanoMIPs) have proven to be a valid alternative to antibodies (Vlatakis et al., 1993) in numerous diagnostic techniques such as enzyme-linked and fluorometric assays for a large variety of analytes (Chianella et al., 2013; Piletsky et al., 2017; Smolinska-Kempisty et al., 2017). NanoMIPs offer numerous advantages when compared with antibodies, notably their ability to bind small molecules, which are often not immunogenic (Wadhwa et al., 2015). Interest in nanoMIPs is growing rapidly due to the ability to imprint a large variety of chemically and structurally different molecules (Piletska et al., 2004; Kamra et al., 2015;

Chantada-Vázquez et al., 2016), as well as complex structures such as proteins (Guerreiro et al., 2014; Pluhar et al., 2015).

Optical fiber sensors (OFS) can be miniaturised, produced at low cost, can be suitable for remote sensing, have multiplexing capability and are immune to electromagnetic interference. OFS are popular in sensing of biochemical analytes such as glucose (Shukla et al., 2017), bacteria (Slavik et al., 2002), antibodies (Liu et al., 2018) and DNA (Huang et al., 2015) owing to their high sensitivity. The ability of label-free detection is one of the distinctive features of OFS, and optical fiber-based surface Plasmon resonance (SPR) (Wang et al., 2017), lossy mode resonance (LMR) (Chiavaioli et al., 2018) and optical grating sensors (Liu et al., 2018) are popular label-free detection techniques that detect biomolecular interaction via change of surface refractive index (RI). An optical fiber long period grating (LPG) sensor has a selected electric field coupled from the fundamental core mode into the fiber cladding, and the extended electric field renders sensitivity to refractive index wherein resonance wavelengths of an LPG sensor change correspondingly. The response to RI change can be explained as:

$$\lambda_i = [n_{core} - n_{clad(i)}]\Lambda \quad (1)$$

Where the  $n_{core}$  and  $n_{clad(i)}$  are the effective refractive indexes of fibre core and  $i^{\text{th}}$  cladding mode;  $\Lambda$  is the grating period of LPG sensor. A change of surrounding refractive index essentially alters the  $n_{clad(i)}$  value, and as a result, the resonance wavelengths  $\lambda_i$  changes.

This work reports, to our knowledge, the first demonstration of an optical fibre sensor for detection of carboxyl-fentanyl. An LPG sensor is functionalised with nanoMIPs for detection of carboxyl-fentanyl in aqueous solution. A state-of-art molecular imprinting technique is deployed for producing nanoMIPs that selectively capture carboxyl-fentanyl on the surface of the functionalised LPG sensor. The LPG sensor of selected grating period operates at the phase matching condition near the visible wavelength range providing high RI sensitivity and a reference LPG is used to compensate temperature cross-sensitivity. Such a sensor array configuration addresses a common limit of single LPG sensors that is their strong dependence on temperature variations in the environment. The reported sensor shows high selectivity to carboxyl-fentanyl, is able to detect fentanyl (due to identical binding sites to carboxyl-fentanyl), negligible response to other tested drugs (i.e. cocaine and morphine) or substances present in blood (glucose and albumin).

## 2. Result and discussion

### 2.1. NanoMIPs characterisation

After synthesis, the nanoMIPs are dialysed in distilled water using dialysis membranes (SnakeSkin™ Dialysis Tubing, 10K MWCO, 22 mm) and concentrated down to 0.67 mg/ml, and this stock was used for all subsequent tests. The size distribution of the nanoMIPs was characterised via Dynamic Light Scattering (DLS, Fig.S.1), which showed an average hydrodynamic diameter of  $171 \pm 2$  nm.

The nanoMIPs contain methacrylic acid, therefore they bear carboxyl groups that can be exploited for immobilisation on the optical fibre (functionalised with primary amine groups) via EDC/NHS coupling. Fig. 1 shows the SEM image of nanoMIPs after immobilisation on the optical fibre. The nanoMIPs show spherical shape with variable sizes around 100 nm. In addition, Transmission Electron Microscopy (TEM) analysis was performed on carboxyl-fentanyl nanoMIPs and results are showed in the Figure S2 using JEOL 1400 transmission electron microscope (JEOL, USA) with an accelerating voltage of 80 kV. Images were taken using a Megaview III digital camera. The nanoMIPs show a comparable size to the one detected by SEM ( $89.9 \pm 17.9$  nm). This is slightly lower than DLS as DLS estimates the hydrodynamic size of the particle which tends to be larger than the dry size of a polymeric particle (Bootz et al., 2004). This is because the nanoMIPs presented in this work

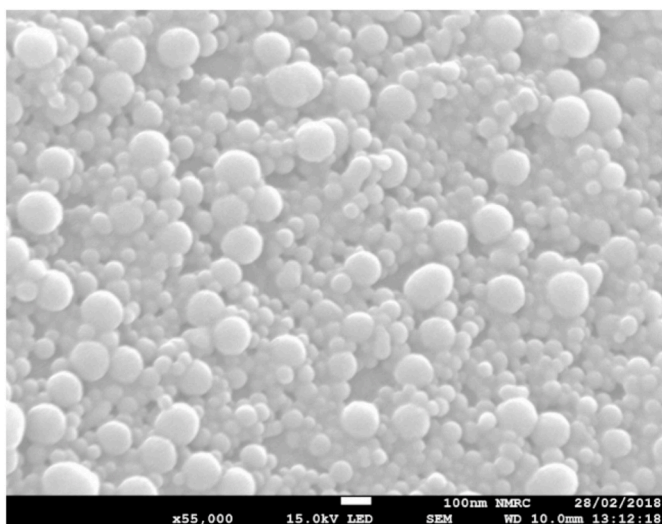


Fig. 1. SEM image of nanoMIPs immobilised on the surface of the optical fibre. Scale bar = 100 nm.

are hydrogels (with low crosslinking degree) which – by definition – would swell in solution, hence leading to an apparent larger size when measured by DLS.

## 2.2. Temperature calibration

At the phase matching condition, the attenuation band of an LPG sensor at a specific cladding mode initially appears as one broad band which continues to grow and finally splits into two coupled bands as

refractive index continues to increase (Xuewen et al., 2002). The coupled dual bands will shift in opposite directions in response to external perturbations such as temperature or refractive index changes. The wavelength separation of the dual bands is therefore used to measure parameters providing a higher sensitivity than a single band. Fig.S.3 demonstrates response of the LPG array sensor to temperature. Both LPG sensors (reference and detection) exhibit a linear increase as temperature increases from 20 °C to 27 °C with sensitivity of 0.49 nm/°C and 0.99 nm/°C, respectively. The coupled dual bands of the two LPGs correspond to the cladding mode LP<sub>019</sub> which is determined by simulation with software *Optigrating* with a model built close to the fabricated sensor (result shown in the supplementary data, Fig.S.4). The detection LPG (nanoMIPs coated) shows a higher sensitivity that is twice of that of the reference LPG (bare). The higher sensitivity is because the detection LPG with a higher grating period is closer to its phase matching turning point than that of reference LPG, where the highest sensitivity is achieved (Xuewen et al., 2002). The contribution of coated nanoMIPs to the high thermal sensitivity of the detection LPG is considered less of importance in this case due to the high temperature stability of MIPs (Refaat et al., 2019). To subtract the temperature effect from the detection LPG sensor, the following equation can be applied:

$$\Delta\lambda = \Delta\lambda_{det} - 2 \times \Delta\lambda_{ref} \quad (2)$$

Where  $\Delta\lambda$  is the wavelength shift induced by the binding,  $\Delta\lambda_{det}$  and  $\Delta\lambda_{ref}$  is the wavelength shift of the detection LPG and reference LPG, respectively.

## 2.3. Sensor measurement

A bare LPG exhibits a wavelength shift of about 0.2 nm when immersed into 1000 ng/mL of the prepared carboxyl-fentanyl solution. The magnitude of wavelength shift is less than its noise level (~0.3 nm)

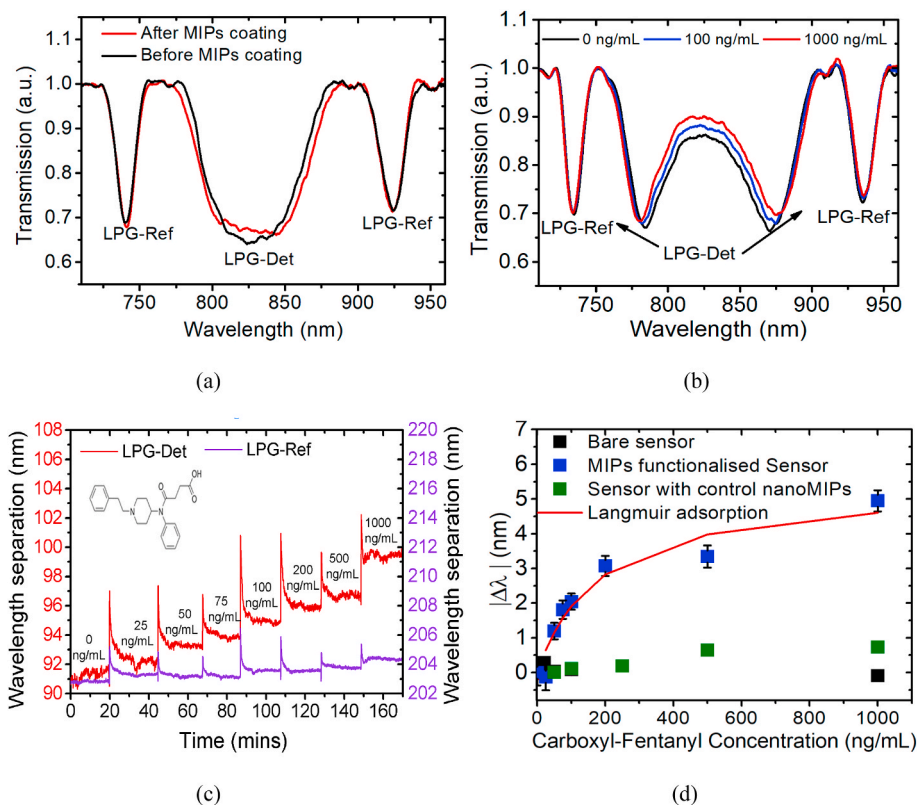


Fig. 2. (a) Transmission spectra of the LPG array in air before and after nanoMIPs coating; (b) Transmission spectra of the LPG array in different concentrations of carboxyl-fentanyl solution. (c) Dynamic response of the LPG array to different concentrations of carboxyl-fentanyl; signal is taken as wavelength separation of the dual bands of LP<sub>019</sub>. (d) Wavelength shift of LP<sub>019</sub> as a function of carboxyl-fentanyl concentration after subtracting temperature contribution.

in a blank sample (solvent only), suggesting that the contribution of bulk refractive index of the fentanyl solution is negligible (result not shown). Fig. 2a illustrates the transmission spectrum of the LPG array at cladding mode of LP<sub>019</sub> before and after attaching nanoMIPs (surrounding medium is air). It is clear that the reference LPG (LPG-Ref) shows a negligible change in its attenuation bands. The attenuation band of the detection LPG (LPG-Det) in the same cladding mode, on the other hand, shows a further development with the band at phase matching condition separating further indicating the attachment of nanoMIP as a result of the increase of surface RI and effective thickness of the fibre. The transmission spectrum of the LPG array in different concentrations of carboxyl-fentanyl solution is shown in Fig. 2b, in which the dual bands of the detection LPG exhibits an opposite wavelength shift in response to binding of carboxyl-fentanyl, as a result of increase of surface refractive index. The reference LPG, on the other hand, remains relatively stable as carboxyl-fentanyl concentration increases.

The wavelength separation of the dual bands of the two LPGs is illustrated in Fig. 2c as a function of time during the measurement. There is a clear step change for the detection LPG (red colour) that follows the step increase of the concentration of carboxyl-fentanyl in solution from 0 to 1000 ng/mL. The reference LPG (purple colour) also shows certain levels of wavelength change most likely due to temperature fluctuation between solutions. Fig. 2d shows the wavelength shift of the detection LPG after subtracting the temperature effect from the reference LPG by using Eq. (2). The wavelength shift is thus the response solely to binding of carboxyl-fentanyl. The wavelength change exhibits a gradual saturation as the increase of the concentration indicating the gradual saturation of the capture sites. The data fits well with the Langmuir adsorption isotherm with a coefficient of determination value  $R^2 = 0.9629$  ( $p < 0.05$ ). The binding constant and maximum wavelength shift are determined as  $0.0053 \text{ (ng/mL)}^{-1}$  ( $2.03 \text{ }\mu\text{M}^{-1}$ ) and 5.4 nm, respectively. The minimum detectable concentration of carboxyl-fentanyl in the experiment is 50 ng/mL which corresponds to a wavelength shift of  $1.20 \pm 0.2 \text{ nm}$ . The biggest wavelength shift is observed as  $4.95 \pm 0.3 \text{ nm}$  at the concentration of 1000 ng/mL. Compared to the nanoMIPs functionalised sensor, the bare sensor (second LPG array) which is used as a baseline sensor exhibits no shift in its wavelength after compensating temperature effect (black point in Fig. 2d). This result also suggests that wavelength shift in the nanoMIPs functionalised sensor is caused by surface refractive index changes induced by carboxyl-fentanyl binding rather than temperature or bulk refractive index. The concept of bulk refractive index and surface refractive index is explained in depth by Chiavaioli et al (Chiavaioli et al., 2017). The control sensor that was coated with control polymer particles exhibits a small increment in wavelength ( $\sim 0.7 \text{ nm}$ ) at high concentration, indicating that there is a certain level of non-specific adsorption but the signal is far less than in the imprinted sensor.

#### 2.4. Cross-selectivity test

Selectivity is particularly important for biosensors as clinical samples such as blood serum usually contain a variety of substances including large molecules such as proteins or small molecules such as glucose. High selectivity ensures a biosensor responds to the presence of interferents to a lesser extent compared to the target analytes. Fig. 3a shows the developed carboxyl-fentanyl sensor response to drugs typically found in blood samples of fentanyl and fentanyl analogues overdose victims, such as morphine, and cocaine (Pearson et al., 2015; Gill et al., 2013). Albumin is the most abundant protein presents in human blood serum. The cross-selectivity of the developed carboxyl-fentanyl sensor is tested separately against BSA and glucose solution ( $1 \text{ }\mu\text{g/mL}$  in distilled water) which are the two most abundant interfering substances present in blood serum. The result shows that the sensor does not respond to the presence of glucose and only about half nanometer wavelength shift in the presence of BSA (Fig. 3b). The wavelength shift is likely to be caused by non-specific adsorption of BSA on the nanoMIPs particles.

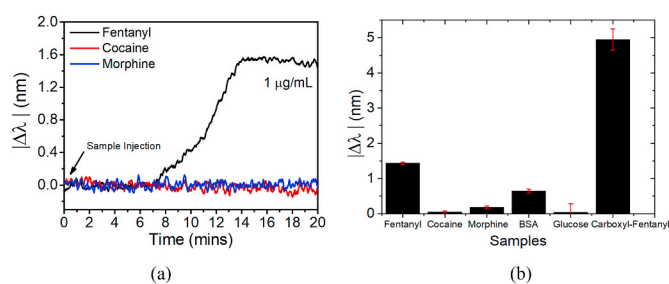


Fig. 3. (a) Real-time response of the developed sensor to three different drugs (fentanyl, morphine and cocaine in methanol), at a concentration of  $1 \text{ }\mu\text{g/mL}$ . (b) Sensor response to different substances ( $1 \text{ }\mu\text{g/mL}$ ).

Remarkably, the sensor does show greater selectivity for the two small molecules cocaine and morphine and, even more interestingly, is able to distinguish between very structurally similar compounds as fentanyl and carboxyl fentanyl.

Selectivity over carboxyl-fentanyl is likely due to the monomers capability of arranging around the template during the imprinting process and forming a specific binding site by means of not covalent interactions. The monomers part of the polymerisation mixture capable of hydrogen bonding (e.g. methacrylic acid) can interact with the carbonyl of carboxyl-fentanyl during the imprinting process, thus creating a specific interaction. Therefore, the resulting MIP would be able to recognise that carbonyl group imprinted in the first place. The LPG of the nanoMIPs coated grating operates at the phase-matching condition providing high RI sensitivity to measure small RI change induced by carboxyl-fentanyl binding. A reference LPG within the array enables temperature compensation during measurements. This approach addresses a common issue of these type of sensors that is temperature cross-sensitivity, thus strict temperature control is no longer needed. Resolution for temperature measurement of the detection and reference LPG are  $0.34 \text{ }^\circ\text{C}$  and  $0.17 \text{ }^\circ\text{C}$ , respectively. This suggests that the temperature fluctuation within  $0.34 \text{ }^\circ\text{C}$  will not be removed from the detection LPG (equivalent wavelength shift is  $\sim 0.33 \text{ nm}$ ) due to the lower temperature sensitivity of the detection LPG. Therefore, the resolution of the LPG array sensor for detection of carboxyl-fentanyl is defined as  $0.33 \text{ nm}$  which tolerates the temperature fluctuation despite the spectral resolution of the spectrometer being  $0.17 \text{ nm}$ .

The MIPs functionalised sensor is further deployed to detect carboxyl-fentanyl in human serum. The results demonstrate that the sensor responds to the presence of carboxyl-fentanyl in serum with an increase in wavelength separation with increase of carboxyl-fentanyl concentration (Fig. S6a). The increase of wavelength separation in PBS washing solution after each exposure in serum sample also confirms the attachment of carboxyl-fentanyl on the sensor surface. In contrast, the sensor's subsequent exposure to a blank serum sample shows no change at each exposure (Fig. S6b).

#### 2.5. Comparison with existing method

A comparison of different approaches is shown in Table 1. Although some of the laboratory based instruments provide better performance, they are impractical for real time routine forensics due to size; longer testing times; expense of equipment and operator training. The optical fibre nanoMIP sensor provides the potential for a new point of use platform that can be rapidly adapted for different molecules and multiplexed sensing.

One of the most concerning issues in the forensic field is the lack of drug detection due to a large time window between the discovery of a new designer drug and its routine detection in hospitals and police stations (Harper et al., 2017). The short production time of nanoMIPs (average of 4 weeks synthesis and characterisation), combined with its flexibility to imprint many types of molecules, is a considerable

**Table 1**

A summary of available technologies for detection of fentanyl or fentanyl analogues.

Existing sensing technologies for fentanyl/fentanyl analogues	Pros	Cons	Ref
Radioimmunoassay	<ul style="list-style-type: none"> <li>• <b>Quantitative:</b> high sensitivity and specificity</li> <li>• <b>High throughput:</b> ability to run multiple samples</li> </ul>	<ul style="list-style-type: none"> <li>• <b>Cost:</b> radiolabelling is required increasing the cost</li> <li>• <b>Time required for analysis:</b> radiolabelling required, pre-treatment of the sample required, multi-step protocol, no real-time measurement,</li> <li>• <b>Ease of use:</b> intermediate-advanced expertise required</li> </ul>	Michiels et al. (1977)
Liquid chromatography-mass spectrometry	<ul style="list-style-type: none"> <li>• <b>Quantitative:</b> high sensitivity and specificity</li> <li>• <b>High throughput:</b> Analysis of mixture compounds for metabolism study</li> </ul>	<ul style="list-style-type: none"> <li>• <b>Cost:</b> bulky and costly detection device</li> <li>• <b>Time required for analysis:</b> multi-steps of sample preparation</li> <li>• <b>Ease of use:</b> intermediate-advanced expertise required</li> </ul>	(Kanamori et al., 2021; Busardò et al., 2019)
TD-DART-MS & IMS	<ul style="list-style-type: none"> <li>• <b>Quantitative:</b> high sensitivity</li> <li>• <b>High throughput:</b> analysis of mixture compounds</li> <li>• <b>Time required for analysis:</b> rapid detection</li> </ul>	<ul style="list-style-type: none"> <li>• <b>Costly:</b> Bulky and costly detection device</li> </ul>	Sisco et al. (2017)
Surface-enhanced Raman spectroscopy	<ul style="list-style-type: none"> <li>• <b>High throughput:</b> analysis of mixture compounds</li> <li>• <b>Time required for analysis:</b> rapid detection method</li> <li>• <b>Ease of use:</b> simple sample preparation process, Basic-advanced (depending on model)</li> </ul>	<ul style="list-style-type: none"> <li>• <b>Costly:</b> Bulky and costly detection device</li> </ul>	Haddad et al. (2018)
Electrochemical glove-based sensor	<ul style="list-style-type: none"> <li>• <b>Cost:</b> Low-cost</li> <li>• <b>Ease of use:</b> intermediate-portable device</li> <li>• Direct measurement</li> </ul>	<ul style="list-style-type: none"> <li>• <b>Sensitivity:</b> Lower sensitivity than laboratory-based equipment</li> <li>• <b>High throughput:</b> NO, single measurement</li> </ul>	Barfidokht et al. (2019)
MIPs functionalised LPG sensor	<ul style="list-style-type: none"> <li>• <b>Quantitative</b></li> <li>• <b>Ease of use:</b> basic-intermediate-</li> </ul>	<ul style="list-style-type: none"> <li>• <b>Sensitivity:</b> Lower sensitivity than</li> </ul>	This work

**Table 1 (continued)**

Existing sensing technologies for fentanyl/fentanyl analogues	Pros	Cons	Ref
	<ul style="list-style-type: none"> <li>• compact/mobile device</li> <li>• Direct measurement</li> <li>• <b>Cross selectivity:</b> very low cross selectivity with analogues</li> <li>• <b>Cost:</b> Low-cost</li> <li>• Immune to EMI</li> </ul>	<ul style="list-style-type: none"> <li>• laboratory-based equipment</li> <li>• <b>High throughput:</b> NO, single measurement</li> </ul>	

advantage over the techniques previously described. NanoMIPs can be manufactured and integrated in the device reported in a short period of time still maintaining a high level of sensitivity, as demonstrated in Section 2.3.

The integration of the flexibility of nanoMIPs to optical fibre technology provides the basis for producing an interchangeable device for different detection purposes. The device, currently demonstrated to measure one compound at the time, could easily be upgraded to a multiplexing platform by functionalising more than one optical fibre, or LPG, with nanoMIPs imprinted for different molecules, analogues of the same drug, as well as structurally different molecules (e.g. peptides or proteins), achieving the simultaneous monitoring of a multitude of parameters for a more complete diagnostic picture, previously identified as the ultimate goal of the diagnostic field (Tighe et al., 2015).

### 3. Experimental

Traditional imprinting methods typically require several days due to the need for multiple time-consuming purification steps (Cirillo et al., 2009). An innovative solid-phase synthesis which overcomes these problems is becoming more popular, as it reduces the speed of manufacturing and requires very little post-synthesis purification (Guerreiro et al., 2009). This approach can be successfully applied in both organic (UV-triggered process) and water (persulfate-initiated polymerisation) solutions; aqueous polymerisations have shown to be more efficient in imprinting peptides and proteins (Poma et al., 2013, 2014), whereas organic ones work better for small molecules (Moczko et al., 2013; Basozabal et al., 2014). Indeed, the organic polymerisation was chosen for the imprinting of carboxyl-fentanyl. The organic photopolymerisation used in this work employs *N,N'*-diethyldithiocarbamic acid benzyl ester as initiator. This kind of initiator can act as an initiator, transfer agent and terminator (Iniferter). Iniferters generate one radical (dithiocarbamyl) after the decomposition step which can terminate the growth of the polymer chains in solution, reforming the initial C-S bond. Therefore, the product formed after termination can further generate a new propagating radical upon application of the stimulus triggering the polymerisation (Lim et al., 2003). In this way, sequential polymerisations with other monomers can be re-initiated, in order to tailor properties or functionalities of the synthesised particles (Guerreiro et al., 2009) (Takayuki, 2000). Moreover, in contrast to conventional radical polymerisation, the iniferter-based living polymerisation proceeds at low rate without auto acceleration phenomena, allowing a better control over some parameters such as the polymer chain length and the particle size (Kannurpatti et al., 1996).

#### 3.1. Silanization of solid-phase support

A solid-phase approach described by Canfarotta et al. (2016) was adapted for nanoMIPs synthesis. The surface of glass beads (100 g) was activated by boiling in sodium hydroxide (4 M, 80 mL) for 15 min prior to washing with water (5 × 2 L). The beads were subsequently placed in

a solution of sulphuric acid (50%, 40 mL) for 60 min before again being washed with water ( $3 \times 2$  L) and incubated in buffer (PBS 10 mM, 400 mL) for 5 min. Further water washes ( $10 \times 2$  L) were performed to ensure the final pH was between 6 and 8. The solid phase was dried by washing with acetone ( $3 \times 240$  mL) and placing under vacuum, before leaving in an oven ( $150^\circ\text{C}$ ) for 60 min. Activated beads were incubated in a solution of toluene (40 mL) with (3-aminopropyl)triethoxysilane (1.172 mL, 5.418 mmol) and 1,2-bis(triethoxysilyl)ethane (0.96 mL, 2.59 mmol) overnight at  $80^\circ\text{C}$ . Beads were subsequently washed with toluene ( $3 \times 450$  mL), ethanol ( $3 \times 450$  mL), and acetone ( $5 \times 450$  mL) to remove any residual silane, before drying under vacuum and further oven drying for 60 min at  $150^\circ\text{C}$ .

The presence of  $\text{NH}_2$  groups was assessed using ninhydrin test. A sample of dry glass beads ( $1 \times 3$  g of glass beads) was incubated with a ninhydrin solution (2 mL, 6 mM in EtOH) for 180 min, at  $60^\circ\text{C}$ . The absorbance was then read at  $580 \pm 3$  nm. A surface coverage of  $0.967 \mu\text{mol NH}_2$  per gram of glass beads was achieved.

EDC/NHS coupling was used to covalently attach the template of interest to the surface of the glass beads. Due to the lack of functional groups available in the native structure of fentanyl for coupling to the solid support, an analogue containing a carboxyl group (Fig.S.5) was instead used, allowing immobilisation to be performed using a straightforward EDC/NHS coupling strategy.

### 3.1.1. Carboxyl-fentanyl synthesis

The relevant chemical reactions involved in synthesis of carboxyl-fentanyl are illustrated in Fig. 4 and the process is described in detail below.

**3.1.1.1. *N*-[1-(2-phenethyl)-4-piperidinyl]aniline (2).** This compound was prepared following the method reported by Valdez et al. (2014): Aniline (2.06 g, 22 mmol) and dichloromethane (60 mL) were added to a 3-necked round-bottomed flask equipped with stopper,  $\text{CaCl}_2$  guard tube and a dropping funnel. The contents were stirred and cooled (ice-bath) and acetic acid (1.25 mL) was added dropwise to the mixture. This was followed by a further 10 mL of dichloromethane to rinse the dropping funnel before the addition of a solution of *N*-phenethylpiperidin-4-one (1) (4.5 g, 22 mmol) in dichloromethane (15 mL). When addition was complete, sodium triacetoxyborohydride (7.025 g, 33 mmol) was added in small portions to the mixture. When addition was complete, the ice

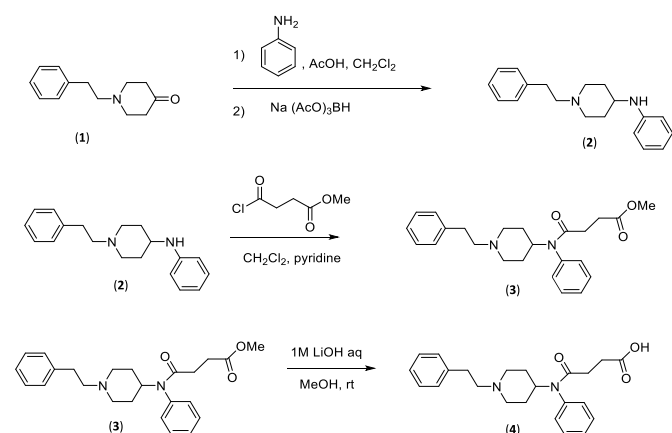


**Fig. 4.** Schematic illustration of synthesis of carboxyl-fentanyl, *N*-[1-(2-phenethyl)-4-piperidinyl]aniline (2) was prepared with the addition of aniline and dichloromethane to *N*-phenethylpiperidin-4-one (1). Methyl 4-oxo-4-(phenyl-[1-(2-phenylethyl)-4-piperidinyl] amino) butanoate (3), was prepared by the addition of  $\text{CaCl}_2$  and *N*-[1-(2-phenethyl)-4-piperidinyl]aniline in dry dichloromethane to which was added pyridine. For the synthesis of 4-oxo-4-(phenyl-[1-(2-phenylethyl)-4-piperidinyl] amino) butanoic acid (4) (carboxyl-fentanyl) the hydrolysis of (3) was carried out. The pure fraction was also obtained as an amorphous solid.

bath was removed and the mixture stirred at room temperature overnight. After the overnight stirring, methanol (25 mL) was added to destroy any excess of reducing agent and the reaction mixture was transferred to a 1 L separating funnel and the acid neutralised by the addition of saturated  $\text{NaHCO}_3$  solution (approx 200 mL). When  $\text{CO}_2$  evolution had ceased, the clear yellow lower organic layer was separated and the aqueous layer was extracted with more  $\text{CH}_2\text{Cl}_2$  (10 mL). After setting aside the aqueous layer, the combined organics were returned to the separating funnel and washed with brine ( $3 \times 25$  mL) and the organics were dried ( $\text{MgSO}_4$ ), filtered and evaporated to give a solid residue. This was recrystallized from hexanes to yield 4.1413g (67%) of an off-white solid. The NMR ( $^1\text{H}$  and  $^{13}\text{C}$ ) was identical to the literature spectra (Valdez et al., 2014) with no impurities. Subsequent concentration of the mother liquor and recrystallization gave a second batch of 0.4013g, giving an overall yield of 4.5g (73%).  $^1\text{H}$  NMR  $\text{CDCl}_3$  (500 MHz) 7.28–7.31 (m, 2H), 7.20–7.22 (m, 3H), 7.17 (t,  $J = 7\text{Hz}$ , 2H), 6.68 (t,  $J = 7\text{Hz}$ , 1H), 6.60 (d  $J = 8\text{Hz}$ , 2H), 3.52 (br, 1H), 3.32 (m, 1H), 2.80–2.84 (m, 2H), 2.60–2.63 (m, 2H), 2.21 (t,  $J = 11\text{Hz}$ ), 2.09 (d,  $J = 12\text{Hz}$ , 2H), 1.51 (m, 2H).  $^{13}\text{C}$  NMR  $\text{CDCl}_3$  (125.77 MHz) 147.12, 140.43 ( $2 \times$  quat.), 129.37, 128.74, 128.44, 126.09, 117.23, 113.26 ( $6 \times$  aromatic CH), 60.73, 52.53 ( $2 \times \text{CH}_2$ ), 49.95 (CH), 33.97, 32.63 ( $2 \times \text{CH}_2$ ).

**3.1.1.2. Methyl 4-oxo-4-(phenyl-[1-(2-phenylethyl)-4-piperidinyl] amino) butanoate (3).** This compound was prepared by the method of Bremer et al. (2016) based on the synthesis of the homologous pentanoate derivative. In a 3-necked flask fitted with stopper,  $\text{CaCl}_2$  guard tube and addition funnel: *N*-[1-(2-phenethyl)-4-piperidinyl]aniline (2 g, 7.14 mmol) was dissolved in dry dichloromethane (50 mL) to which was added pyridine (1.15 mL, 14.2 mmol). The solution was cooled in an ice-bath before the dropwise addition, with stirring, of methyl succinyl chloride (1.03 g, 7.8 mmol) in dry dichloromethane (20 mL). After addition of the acyl chloride, the reaction was stirred at  $0^\circ\text{C}$  for 5 min before removing from the ice bath and stirring for 4h at room temperature. The reaction was quenched by the addition of a saturated aqueous solution of  $\text{NaHCO}_3$  and the contents of the flask transferred to a separating funnel. The dichloromethane layer was separated and the aqueous layer extracted with ethyl acetate ( $3 \times 25$  mL). The combined organic extracts were washed once with brine, separated, dried ( $\text{MgSO}_4$ ) and evaporated to give a pale yellow oil. The product was obtained as colourless crystals from hexanes, 1.88 g, (67%).  $^1\text{H}$  NMR  $\text{CDCl}_3$  (400 MHz) 7.35–7.43 (m, 3H), 7.23–7.27 (m, 2H), 7.12–7.19 (m, 5H), 3.66 (s, 3H), 3.0–3.02 (m, 2H), 2.71–2.75 (m, 2H), 2.51–2.58 (m, 4H), 2.20 (t,  $J = 6.5\text{Hz}$ , 2H), 2.15 (d,t,  $J = 2\text{Hz}$ ,  $J = 12\text{Hz}$ , 2H), 1.79–1.83 (m, 2H), 1.44 (tt,  $J = 4\text{Hz}$ ,  $J = 12\text{Hz}$ , 2H).  $^{13}\text{C}$  NMR  $\text{CDCl}_3$  (100.62 MHz) 173.57, 171.01 ( $2 \times$  carbonyl), 140.15, 138.43 ( $2 \times$  quat), 130.45, 129.44, 128.63, 128.49, 128.39, 126.04 ( $6 \times$  aromatic CH), 60.35, 53.00 ( $2 \times \text{CH}_2$ ), 52.44, 51.65, 33.71, 30.40, 30.10, 29.21 ( $4 \times \text{CH}_2$ ).

**3.1.1.3. 4-oxo-4-(phenyl-[1-(2-phenylethyl)-4-piperidinyl] amino) butanoic acid (4) (hydrolysis method) (carboxyl-fentanyl).** The hydrolysis of (3) was also carried out according to Bremer (Bremer et al., 2016). The methyl ester (1.5 g, 3.8 mmol) was dissolved in methanol (30 mL) and aqueous  $\text{LiOH}$ , 1M, (7.6 mL) was added and the mixture stirred at room temperature overnight. The mixture was washed with hexane, then acidified with HCl. The acidified solution was extracted with ethyl acetate ( $3 \times 25$  mL) and the combined organics dried ( $\text{MgSO}_4$ ) and evaporated to give a colourless foamy solid (0.84 g). Attempts to crystallise the products were unsuccessful despite reports of crystallisation from ethyl acetate (Vardanyan et al., 2011), methanol (Nichol et al., 2010), or a benzene-hexane mixture (Henderson et al., 1975). As crystallisation might be inhibited by an impurity, the product was purified by column chromatography on silica gel, from 5%  $\text{MeOH}:\text{CH}_2\text{Cl}_2$  to 10%  $\text{MeOH}:\text{CH}_2\text{Cl}_2$ . A pure fraction was obtained by combining fractions containing the lower of three spots (tlc, silica, 1:9  $\text{MeOH}:\text{CH}_2\text{Cl}_2$ ). The pure fraction (0.46 g) was also obtained as an amorphous solid. (32 %).

$^1\text{H}$  NMR  $\text{CD}_3\text{OD}$  (400 MHz) 7.57–7.49 (m, 3H), 7.36–7.32 (m, 4H), 7.28–7.25 (m, 3H), 4.80 (tt,  $J = 12.9$  Hz, 4.3 Hz, 1H) 3.65 (br d,  $J = 12.5$  Hz, 2H), 3.30–3.25 (m, 2H), 3.20–3.13 (m, 2H), 3.03–2.98 (m, 2H), 2.54 (t,  $J = 6.5$  Hz, 2H), 2.23 (t,  $J = 6.5$  Hz, 2H), 2.15 (br d,  $J = 13.7$  Hz, 2H), 1.79–1.68 (m, 2H).  $^{13}\text{C}$  NMR  $\text{CDCl}_3$  (125.77 MHz) 175.71, 172.21, 136.21, 130.08, 129.70, 129.34, 128.93, 128.77, 127.23, 53.44, 51.86, 50.65, 50.56, 30.30, 29.95, 29.34, 27.49.

### 3.1.2. Carboxyl-fentanyl immobilisation on glass beads

Silanised glass beads (60 g) were incubated with the solution of EDC/NHS/template in PBS (24 mL, 10 mM) at 0.1 mg/mL of carboxyl-fentanyl (6.29  $\mu\text{mol}$ ). Prior to the incubation with glass beads, the  $-\text{COOH}$  groups of the carboxyl-fentanyl are activated by adding EDC (10 times molar excess, 62.9  $\mu\text{mol}$ ) and NHS (15 times molar excess, 94.5  $\mu\text{mol}$ ) to a solution of MES buffer (10 mM, pH 5–6) for 10 min. The activated template solution is then added to glass beads in PBS and incubated at room temperature for 4h prior to washing with water ( $10 \times 24$  mL), then acetone ( $3 \times 24$  mL) and eventually dried under vacuum.

### 3.1.3. NanoMIPs synthesis

The process of synthesising nanoMIPs is illustrated in Fig. 5. Polymerisation mixture consisting of MAA (2.15 g, 24.97 mmol), HEMA (0.435 g, 3.34 mmol), styrene (0.174 g, 1.67 mmol), EGDMA (3.24 g, 16.35 mmol), TRIM (3.24 g, 9.57 mmol) PEMPT (0.18 g, 0.37 mmol) N, N-diethylthiocarbamic acid benzyl ester (0.75 g, 3.13 mmol) tri-fluoroethyl methacrylate (0.515 g, 3.06 mmol), fluorescein-*N*-acrylate (0.025 g, mmol) was prepared in ACN (12 mL) and purged with nitrogen for 17 min at  $0^\circ\text{C}$  under exclusion of light. Following this, the polymerisation mixture was added to the derivatised beads (30 g) (Fig. 5a) and polymerisation initiated using UV light for 1 min and 45 s (Fig. 5b). The beads were subsequently washed with ACN ( $10 \times 30$  mL) at  $0^\circ\text{C}$  to remove unreacted monomer and low-affinity polymer before eluting high-affinity nanoMIPs with hot ACN (100 mL,  $60^\circ\text{C}$ ) (Fig. 5c and d).

Control nanoMIPs were produced using the same protocol as the described above, with a small model peptide used as target molecule. It should be noted that it is not possible to produce NIPs with the same size (and hence surface area) by solid-phase imprinting: given the MIPs are produced around the template immobilised on the solid-phase, producing NIPs without any template immobilised on the solid-phase is not possible. In order to address this and account for any potential non-specific adsorption of the template on the MIPs, a control MIP was produced, which is essentially a polymer with identical composition to the MIPs, only imprinted for a non-related molecule, such that the MIPs can be collected after the cold washes. In this case, the “template” acts as an “anchor” such that control MIPs can be harvested – following the exact same protocol used for the target MIPs.

Non-specific binding would derive from the outer polymer layer on the MIP. So, as long as the polymer composition between target and control MIPs is kept constant and the production process is the same, the control MIP would be the equivalent of a NIP and would therefore give an indication of any potential non-specific binding.

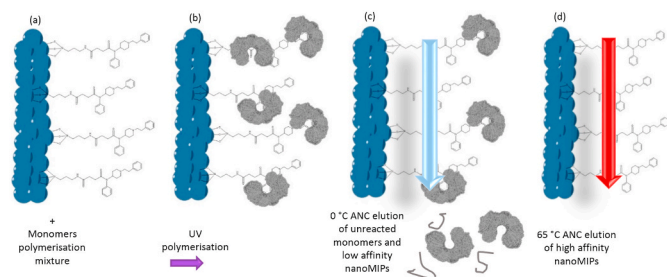


Fig. 5. Schematic representation of solid-phase synthesis of carboxyl-fentanyl imprinted nanoMIPs.

### 3.1.4. Post-synthesis characterisation

After collection, the high-affinity nanoMIPs were evaporated down to 2 mL, 8 mL HPLC water added and dialysed overnight using Snake-Skin 10 K MWCO dialysis membranes. Nanoparticle size was determined by DLS using a Zetasizer Nano (Nano-S, Malvern Instruments, UK). Prior to DLS measurements, samples were subjected to sonication for 2 min, vortexed for 30 min, and measurements performed at  $25^\circ\text{C}$ .

### 3.2. Functionalisation of the LPG sensor

An LPG array with two LPGs located closely (1.5 cm length each with  $\sim 1$  cm gap in between) on a single fibre is fabricated through UV irradiation on a boron-doped photo-sensitive optical fibre (PS750, Fibre-core, UK). A frequency quadrupled Nd:YAG laser emitting at 266 nm (Continuum minilite I) is the laser source used to inscribe a periodic grating structure on the optical fibre through custom made steel alloy amplitude masks. The two LPGs having grating period of 111.5  $\mu\text{m}$  and 110.0  $\mu\text{m}$  are used as detection and reference LPG respectively.

The functionalisation of LPG is conducted by immobilizing nanoMIPs on the LPG sensor surface. This process involves two steps as illustrated in Fig. 6a:

**Silanization of LPG surface:** the detection LPG is initially treated with 1 wt% ethanolic KOH solution (ethanol/water = 3:2, v/v) for 30 min to etch the surface with  $-\text{OH}$  group. After washing with deionized water (15 M $\Omega$  cm) and drying with  $\text{N}_2$ , the LPG is then immersed into freshly prepared APTES (2% v/v, APTES in ethanol) for 20 min. After washing with ethanol and water, the LPG is placed into a pre-heated oven at a

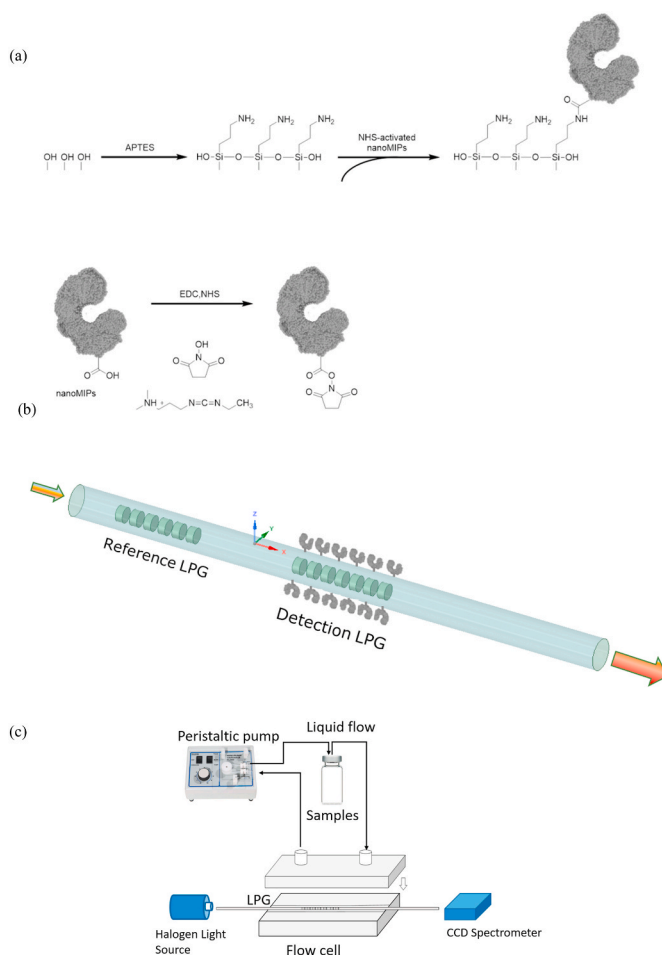


Fig. 6. (a) Surface functionalisation process involved in the nanoMIPs coating; (b) Schematic illustration of an LPG array; (c) Flow system for measuring of analytes.

temperature of 120 °C for 20 min to condense the chemical bonds (-Si-O-Si-) and remove water molecules from the surface.

**Fentanyl nanoMIPs immobilisation:** a 150 µL aliquot of the sonicated nanoMIPs solution in water is added into 400 µL of MES buffer (0.1 M, pH = 5.6) containing 0.4 mg of EDC and 1 mg of NHS, and stirred 15 min at room temperature (22 °C). Subsequently, 175 µL of carbonate buffer (pH = 11) are added to the solution to increase the pH to about 7; the prepared LPG is then incubated overnight at room temperature. Afterwards, the LPG is washed with distilled water to remove loosely bound nanoMIPs, and then immersed into a carbonate buffer (pH = 9.2) for 2 h to hydrolyse remaining NHS-esters and recover the original -COOH groups.

Control nanoMIPs were immobilised on the LPG sensor by using the same protocol used for carboxyl-fentanyl nanoMIPs.

### 3.3. Measurement procedure with the developed OFS

Different concentrations of carboxyl-fentanyl solutions are prepared by dissolving carboxyl-fentanyl into a solvent that contains a mixture of methanol and distilled water in a ratio of 1:3 v/v with a concentration range from 0 to 1000 ng/mL.

For the measurement, the LPG array (shown in Fig. 6b) is subsequently exposed to different concentrations of the prepared carboxyl-fentanyl solution for 20 min, followed by washing with distilled water between each measurement. Meanwhile, a second LPG array with the same grating periods and transmission spectrum to the first array without nanoMIPs coating is used as a baseline sensor. The second LPG array was immersed into different concentrations of the same carboxyl-fentanyl solution to evaluate the effect of bulk refractive index of the testing solution to the response of the LPG array. A halogen light source (Ocean Optics, HL-2000, UK) and a CCD spectrometer (Ocean Optics, HR4000, UK) are employed for launching light into the fibre and detecting the transmission spectrum of the LPGs. Furthermore, a closed-loop microfluidic flow system (Fig. 6c) is adapted for testing the sensor response. For selectivity tests, popular opioid drugs including fentanyl and morphine, and cocaine with the same concentration (1000 ng/mL, in methanol) were used. An in-house made silicone flow cell for hosting LPG is fabricated by casting silicone elastomer (Sylgard® 184) into a 3D printed mould and curing in ambient temperature for two days. The channel in which the LPG lays has an inner diameter of ~1 mm that allows liquid to flow through. A peristaltic pump circulates drug samples to the flow cell at a speed of 0.4 mL/min that produces an optimal liquid flow of ~8 mm/s inside of the flow channel which is experimentally defined by balancing diffusion limit and shear stress as reported in (Huang et al., 2014).

To demonstrate the applicability of such a sensor in real sample, human serum containing different concentrations of carboxyl-fentanyl are prepared by dissolving carboxyl-fentanyl in methanol and further mixing with human serum (the volume ratio of serum to methanol is 100:1). The sensor is subsequently exposed to the prepared sample from low to high concentrations followed by washing with PBS buffer.

## 4. Conclusion

NanoMIPs imprinted with carboxyl-fentanyl were successfully synthesised and collected via a solid-phase approach. The nanoMIPs (average hydrodynamic diameter of  $171 \pm 2$  nm) are successfully deposited on the surface of an LPG array optical fibre sensor via EDC/NHS coupling.

The LPG array with selected grating periods is fabricated through UV irradiation to provide high RI sensitivity. Experimental results demonstrate that the synthesised nanoMIPs have the capability of rebinding carboxyl-fentanyl and producing a detectable refractive index change which is indicated via a wavelength shift in the LPG array. Interestingly, the developed nanoMIPs-LPG sensor does not respond to blood interferences (BSA and glucose) and similarly sized small molecules (morphine

and cocaine), and most notably shows much higher selectivity for its structurally similar compound fentanyl. Every year new psychoactive substance analogues are brought to the market, often with very small structural changes from the lead compound. The rapid development of these analogues challenges diagnostics to keep pace, therefore making sensor fabrication quickly is pivotal. The results from this work demonstrate the manufacture of a versatile sensor showing low cross-reactivity with analogues and interfering compounds, and with little development time required.

## Funding

This work is funded by the EPSRC Cyclops Healthcare Network (EP/N026985/1), MIP diagnostics Ltd and European Regional Development Fund.

## CRediT authorship contribution statement

**LiangLiang Liu:** Formal Investigation, analysis and original draft. **Fabiana Grillo:** Formal Investigation, analysis and original draft. **Francesco Canfarotta:** Methodology, and review & editing. **Michael Whitcombe:** Methodology, Writing - review & editing. **Stephen P. Morgan:** Conceptualization, Funding acquisition, Supervision, and review & editing. **Sergey Piletsky:** Conceptualization, Funding acquisition, Supervision, and review & editing. **Ricardo Correia:** Methodology, and review & editing. **ChenYang He:** Formal Investigation, analysis and original draft. **Andrew Norris:** Conceptualization, Funding acquisition, Supervision, and review & editing. **Serhiy Korposh:** Conceptualization, Funding acquisition, Supervision, and review & editing.

## Declaration of competing interest

The authors declare that they have no known competing financial interests or personal relationships that could have appeared to influence the work reported in this paper.

## Acknowledgement

The authors thank the Nanoscale and Microscale Research Centre (nmRC) at the University of Nottingham for providing access to microscopy facilities.

## Appendix A. Supplementary data

Supplementary data to this article can be found online at <https://doi.org/10.1016/j.bios.2021.113002>.

## References

- ECDMA, 2017. European Drug Report 2017: Trends and Developments, pp. 1–97.
- Armenian, P., et al., 2018. Fentanyl, fentanyl analogs and novel synthetic opioids: a comprehensive review. *Neuropharmacology* 134, 121–132.
- Barfidokht, A., et al., 2019. Wearable electrochemical glove-based sensor for rapid and on-site detection of fentanyl. *Sensor. Actuator. B Chem.* 296, 126422.
- Basozabal, I., et al., 2014. Direct potentiometric quantification of histamine using solid-phase imprinted nanoparticles as recognition elements. *Biosens. Bioelectron.* 58, 138–144.
- Boot, A., et al., 2004. Comparison of scanning electron microscopy, dynamic light scattering and analytical ultracentrifugation for the sizing of poly(butyl cyanoacrylate) nanoparticles. *Eur. J. Pharm. Biopharm.* 57 (2), 369–375.
- Bremer, P.T., et al., 2016. Combatting synthetic designer opioids: a conjugate vaccine ablates lethal doses of fentanyl class drugs. *Angew. Chem. Int. Ed.* 55 (11), 3772–3775.
- Busardo, F.P., et al., 2019. Ultra-high-performance liquid chromatography-tandem mass spectrometry Assay for quantifying Fentanyl and 22 Analogs and Metabolites in whole blood, urine, and hair. *Front. Chem.* 7, 184.
- Campuzano, S., Pedrero, M., Pingarrón, J.M., 2018. Electrochemical nucleic acid-based biosensing of drugs of abuse and pharmaceuticals. *Curr. Med. Chem.* 25 (33), 4102–4118.

- Canfarotta, F., et al., 2016. Solid-phase synthesis of molecularly imprinted nanoparticles. *Nat. Protoc.* 11, 443.
- Chantada-Vázquez, M.P., et al., 2016. Simple and sensitive molecularly imprinted polymer – Mn-doped ZnS quantum dots based fluorescence probe for cocaine and metabolites determination in urine. *Anal. Chem.* 88 (5), 2734–2741.
- Chianella, I., et al., 2013. Direct replacement of antibodies with molecularly imprinted polymer nanoparticles in ELISA—development of a novel assay for vancomycin. *Anal. Chem.* 85 (17), 8462–8468.
- Chiavaoli, F., et al., 2017. Towards a uniform metrological assessment of grating-based optical fiber sensors: from refractometers to biosensors. *Biosensors* 7 (2), 23.
- Chiavaoli, F., et al., 2018. Femtomolar detection by nanocoated fiber label-free biosensors. *ACS Sens.* 3 (5), 936–943.
- Cirillo, G., et al., 2009. Imprinted hydrophilic nanospheres as drug delivery systems for 5-fluorouracil sustained release. *J. Drug Target.* 17 (1), 72–77.
- Crime, U.N.O.d.a., 2017. Fentanyl Analogues - 50 years on, 17.
- Drug Enforcement Administration, D.o.J., 2016. Schedules of controlled substances: temporary placement of butyryl fentanyl and beta-hydroxythiofentanyl into Schedule I. Final order. Federal Reg. 81 (92), 29492.
- Drugs of Abuse Testing Market (Products - Analyzers (Immunoassays, Chromatographic Devices, and Breath Analyzers), Rapid Testing Devices (Urine Testing and Oral Fluid Testing), and Consumables (Fluid Collection Devices); Sample Type: Saliva, Breath, Urine, Blood, and Hair and Sweat; Testing Type - Pain Management Testing, Criminal Justice Testing, and Work Place Screening; End-User: Hospitals, Diagnostic Laboratories, On-The-Spot Testing, and Forensic Laboratories) - Global Industry Analysis, Size, Share, Growth, Trends and Forecast 2017-2025, 2018. Transparency Market Research, p. 219.
- Gill, J.R., Lin, P.T., Nelson, L., 2013. Reliability of postmortem fentanyl concentrations in determining the cause of death. *J. Med. Toxicol.* 9 (1), 34–41.
- Guerreiro, A.R., et al., 2009. Selection of imprinted nanoparticles by affinity chromatography. *Biosens. Bioelectron.* 24 (8), 2740–2743.
- Guerreiro, A., et al., 2014. Influence of surface-imprinted Nanoparticles on trypsin activity. *Adv. Healthc. Mater.* 3 (9), 1426–1429.
- Haddad, A., et al., 2018. Detection and quantitation of trace fentanyl in heroin by surface-enhanced Raman spectroscopy. *Anal. Chem.* 90 (21), 12678–12685.
- Harper, L., Powell, J., Pijl, E.M., 2017. An overview of forensic drug testing methods and their suitability for harm reduction point-of-care services. *Harm Reduct. J.* 14 (1), 52.
- Henderson, G.L., Frincke, J., Leung, C.Y., Torten, M., Benjamini, E., 1975. Antibodies to fentanyl. *J. Pharmacol. Exp. Therapeut.* 192, 489–496.
- Huang, C.J., et al., 2014. SPR bacterial pathogen biosensor: The importance of fluidic conditions and probing depth. *Talanta* 122, 166–171.
- Huang, Y., et al., 2015. High-sensitivity DNA biosensor based on optical fiber taper interferometer coated with conjugated polymer tentacle. *Optic Express* 23 (21), 26962–26968.
- Kamra, T., et al., 2015. Photoconjugation of molecularly imprinted polymer nanoparticles for surface-enhanced Raman detection of propranolol. *ACS Appl. Mater. Interfaces* 7 (49), 27479–27485.
- Kanamori, T., et al., 2021. Detection and confirmation of the ring-opened carboxylic acid metabolite of a new synthetic opioid furanylfentanyl. *Forensic Toxicol.* 39, 114–122.
- Kannurpatti, A.R., et al., 1996. Kinetic and mechanistic studies of iniferter photopolymerizations. *Macromolecules* 29 (23), 7310–7315.
- Kimber, J., et al., 2019. Rising opioid-related deaths in England and Scotland must be recognised as a public health crisis. *Lancet Psychiatr.* 6 (8), 639–640.
- Kowalski, S.R., et al., 1987. Sensitive gas liquid chromatography method for the determination of fentanyl concentrations in blood. *J. Pharmacol. Methods* 18 (4), 347–355.
- Le, A.D., Alzghari, S.K., 2019. Syst. Rev. Clin. Consequences Butyrfentanyl Corresponding analogues. 12 (2), 83.
- Leenaars, M., Hendriksen, C.F.M., 2005. Critical steps in the production of polyclonal and monoclonal antibodies: evaluation and recommendations. *ILAR J.* 46 (3), 269–279.
- Lim, E., Jung, B.-J., Shim, H.-K., 2003. Synthesis and characterization of a new light-emitting Fluorene–Thieno[3,2-b]thiophene-based conjugated copolymer. *Macromolecules* 36 (12), 4288–4293.
- Liu, L., et al., 2018. Highly sensitive label-free antibody detection using a long period fibre grating sensor. *Sensor. Actuator. B Chem.* 271, 24–32.
- Michiels, M., Hendriks, R., Heykants, J., 1977. A sensitive radioimmunoassay for fentanyl. Plasma level in dogs and man. *Eur. J. Clin. Pharmacol.* 12 (2), 153–158.
- Moczko, E., et al., 2013. Surface-modified multifunctional MIP nanoparticles. *Nanoscale* 5 (9), 3733–3741.
- Nichol, G.S., et al., 2010. Proton sharing and transfer in some zwitterionic compounds based on 4-oxo-4-(1-phenethylpiperidin-4-yl)(phenyl)amino)alcanoic acids. *CrystEngComm* 12 (11), 3651–3657.
- O'Donnell, J.K., et al., 2017. Deaths Involving Fentanyl, Fentanyl Analogs, and U-47700-10 States, July-December 2016, vol. 66. *MMWR Morb Mortal Wkly Rep*, pp. 1197–1202, 43.
- Oldenhof, S., et al., 2020. Identification of a novel fentanyl analog: p-Hydroxybutyrylfentanyl. *Drug Test. Anal.* 12 (1), 152–155.
- Organization, W.H., 2016. Butyrfentanyl critical review report. 38th ECDD Agenda item 4.2.
- Pearson, J., et al., 2015. Postmortem toxicology findings of acetyl fentanyl, fentanyl, and morphine in heroin fatalities in Tampa, Florida. *Acad. For. Pathol.* 5 (4), 676–689.
- Piletska, E., et al., 2004. Biotin-specific synthetic receptors prepared using molecular imprinting 504, 179–183.
- Piletsky, S.S., et al., 2017. Development of molecularly imprinted polymers specific for blood antigens for application in antibody-free blood typing. *Chem. Commun.* 53 (11), 1793–1796.
- Pluhar, B., Ziener, U., Mizaikoff, B., 2015. Binding performance of pepsin surface-imprinted polymer particles in protein mixtures. *J. Mater. Chem. B* 3 (30), 6248–6254.
- Poma, A., et al., 2013. Solid-phase Synthesis of molecularly imprinted polymer Nanoparticles with a reusable template – “plastic antibodies.”. *Adv. Funct. Mater.* 23 (22), 2821–2827.
- Poma, A., et al., 2014. Automatic reactor for solid-phase synthesis of molecularly imprinted polymeric nanoparticles (MIP NPs) in water. *RSC Adv.* 4 (8), 4203–4206.
- Prekuc, M.P., Mansky, P.A., Baumann, M.H., 2017. Misuse of novel synthetic opioids: a deadly new trend. *J. Addiction Med.* 11 (4), 256.
- Refaat, D., et al., 2019. Strategies for molecular imprinting and the evolution of MIP nanoparticles as plastic antibodies—synthesis and applications. *Int. J. Mol. Sci.* 20 (24), 6304.
- Rubin, R., 2017. Illicit fentanyl driving opioid overdose deaths. *J. Am. Med. Assoc.* 318 (22), 2174–2174.
- Shaw, L., Dennany, L., 2017. Applications of electrochemical sensors: forensic drug analysis. *Curr. Opin. Electrochem.* 3 (1), 23–28.
- Shukla, S.K., et al., 2017. Optical fibre based non-enzymatic glucose sensing over Cu<sup>2+</sup>-doped polyaniline hybrid matrix. *Sensor. Actuator. B Chem.* 242, 522–528.
- Sisco, E., et al., 2017. Rapid detection of fentanyl, fentanyl analogues, and opioids for on-site or laboratory based drug seizure screening using thermal desorption DART-MS and ion mobility spectrometry. *For. Chem. (Amsterdam, Netherlands)* 4, 108–115.
- Slavik, R., Homola, J., Brynda, E., 2002. A miniature fiber optic surface plasmon resonance sensor for fast detection of staphylococcal enterotoxin B. *Biosens. Bioelectron.* 17 (6), 591–595.
- Smolinska-Kempisty, K., et al., 2017. New potentiometric sensor based on molecularly imprinted nanoparticles for cocaine detection. *Biosens. Bioelectron.* 96, 49–54.
- Staheli, S.N., et al., 2016. Time-dependent postmortem redistribution of butyrfentanyl and its metabolites in blood and alternative matrices in a case of butyrfentanyl intoxication. *Forensic Sci. Int.* 266, 170–177.
- Steuer, A.E., et al., 2017. Studies on the metabolism of the fentanyl-derived designer drug butyrfentanyl in human in vitro liver preparations and authentic human samples using liquid chromatography-high resolution mass spectrometry (LC-HRMS). *Drug Test. Anal.* 9 (7), 1085–1092.
- Takayuki, O., 2000. Iniferter concept and living radical polymerization. *J. Polym. Sci. Polym. Chem.* 38 (12), 2121–2136.
- Tighe, P.J., et al., 2015. ELISA in the multiplex era: potentials and pitfalls. *Proteomics Clin. Appl.* 9 (3–4), 406–422.
- Tiscione, N.B., Wegner, K., 2017. Validation of the Neogen® fentanyl ELISA kit for blood and urine. *J. Anal. Toxicol.* 41 (4), 313–317.
- Valdez, C.A., Leif, R.N., Mayer, B.P., 2014. An efficient, optimized Synthesis of Fentanyl and related analogs. *PLoS One* 9 (9), e108250. <https://doi.org/10.1371/journal.pone.0108250>.
- Vardanyan, R., et al., 2011. Synthesis and biological evaluation of new opioid agonist and neurokinin-1 antagonist bivalent ligands. *Bioorg. Med. Chem.* 19 (20), 6135–6142.
- Vlatakis, G., et al., 1993. Drug assay using antibody mimics made by molecular imprinting. *Nature* 361, 645.
- Wadhwa, M., et al., 2015. Immunogenicity assessment of biotherapeutic products: an overview of assays and their utility. *Biologicals* 43 (5), 298–306.
- Wang, G., et al., 2011. Development of a homogeneous immunoassay for the detection of fentanyl in urine. *Forensic Sci. Int.* 206 (1), 127–131.
- Wang, W., et al., 2017. A label-free fiber optic SPR biosensor for specific detection of C-reactive protein. *Sci. Rep.* 7 (1), 16904.
- Wren, S.P., et al., 2014. Preparation of novel optical fibre-based Cocaine sensors using a molecular imprinted polymer approach. *Sensor. Actuator. B Chem.* 193, 35–41.
- Xu, S., Lin, Z., Bennion, I., 2002. Sensitivity characteristics of long-period fiber gratings. *J. Lightwave Technol.* 20 (2), 255–266.